Available online at www.sciencedirect.com

ScienceDirect

Neuromuscular Disorders 29 (2019) 456–467

www.elsevier.com/locate/nmd

Recessive *MYH7*-related myopathy in two families

Sarah J. Beecroft[a,1,*], Martijn van de Locht[b,1], Josine M. de Winter[b], Coen A. Ottenheijm[b], Caroline A. Sewry[c], Shehla Mohammed[d], Monique M. Ryan[e,f,g], Ian R. Woodcock[g], Lauren Sanders[h], Rebecca Gooding[i], Mark R. Davis[i], Emily C. Oates[j], Nigel G. Laing[a,i], Gianina Ravenscroft[a], Catriona A. McLean[k,l,2], Heinz Jungbluth[m,n,o,2]

[a] *Centre for Medical Research University of Western Australia, Harry Perkins Institute of Medical Research, QEII Medical Centre, Nedlands, Western Australia 6009, Australia*

[b] *Physiology, VU University Medical Center, Netherlands*

[c] *Dubowitz Neuromuscular Centre, UCL Great Ormond Street Institute of Child Health, London, United Kingdom*

[d] *Department of Clinical Genetics, Guy's and St Thomas' Hospital, London SE1 7EH, UK*

[e] *Murdoch Children's Research Institute, Melbourne, Australia*

[f] *Department of Paediatrics, The University of Melbourne, Melbourne, Australia*

[g] *Department of Neurology, The Royal Children's Hospital, Melbourne, Australia*

[h] *Department of Medicine, Southern Clinical School, Monash University, Melbourne, Australia*

[i] *Neurogenetics Unit, Department of Diagnostic Genomics, PathWest Laboratory Medicine, QEII Medical Centre, Nedlands, Australia*

[j] *School of Biotechnology & Biomolecular Sciences, The University of New South Wales, Sydney, Australia*

[k] *Department of Anatomical Pathology, Alfred Hospital, Melbourne, Australia*

[l] *Faculty of Medicine Nursing and Health Sciences, Monash University, Melbourne, Australia*

[m] *Department of Paediatric Neurology, Neuromuscular Service, Evelina's Children Hospital, Guy's & St Thomas' Hospital NHS Foundation Trust, London, UK*

[n] *Randall Division of Cell and Molecular Biophysics, Muscle Signaling Section, King's College, London, UK*

[o] *Department of Clinical and Basic Neuroscience, Institute of Psychiatry, Psychology and Neuroscience (IoPPN), King's College, London, UK*

Received 6 February 2019; received in revised form 2 April 2019; accepted 5 April 2019

Abstract

Myopathies due to recessive *MYH7* mutations are exceedingly rare, reported in only two families to date. We describe three patients from two families (from Australia and the UK) with a myopathy caused by recessive mutations in *MYH7*. The Australian family was homozygous for a c.5134C > *T*, p.Arg1712Trp mutation, whilst the UK patient was compound heterozygous for a truncating (c.4699C > *T*; p.Gln1567*) and a missense variant (c.4664A > *G*; p.Glu1555Gly). All three patients shared key clinical features, including infancy/childhood onset, pronounced axial/proximal weakness, spinal rigidity, severe scoliosis, and normal cardiac function. There was progressive respiratory impairment necessitating non-invasive ventilation despite preserved ambulation, a combination of features often seen in *SEPN1*- or *NEB*-related myopathies. On biopsy, the Australian proband showed classical myosin storage myopathy features, while the UK patient showed multi-minicore like areas. To establish pathogenicity of the Arg1712Trp mutation, we expressed mutant *MYH7* protein in COS-7 cells, observing abnormal mutant myosin aggregation compared to wild-type. We describe skinned myofiber studies of patient muscle and hypertrophy of type II myofibers, which may be a compensatory mechanism. In summary, we have expanded the phenotype of ultra-rare recessive *MYH7* disease, and provide novel insights into associated changes in muscle physiology.

Keywords: Myosinopathy; Muscle physiology; Myosin storage myopathy; MYH7; Next generation sequencing.

1. Introduction

Mutations in *MYH7* cause a wide range of cardiac and skeletal muscle diseases, including both dilated and hypertrophic cardiomyopathy (MIM 613426, MIM192600), left ventricular non-compaction (MIM 613426), dominant

* Corresponding author.
E-mail address: sarah.beecroft@uwa.edu.au (S.J. Beecroft).
[1] These authors contributed equally.
[2] Joint supervision.

https://doi.org/10.1016/j.nmd.2019.04.002
0960-8966/

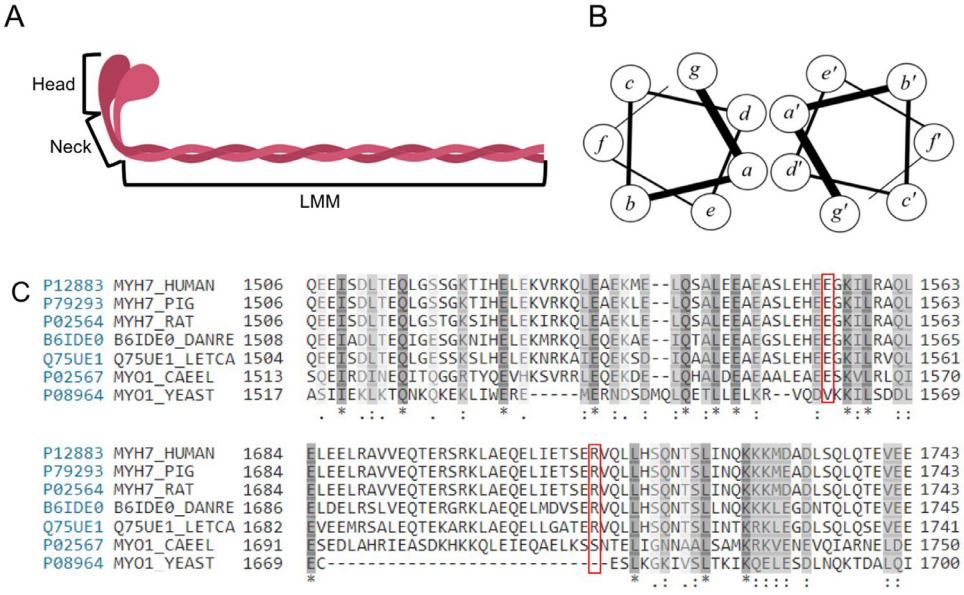

Fig. 1. **(A)** Schematic representation of the MyHC-slow dimer. MyHC-slow contain three main domains from N- to C-terminus: the globular head domain (sub-fragment 1 or S1), the neck domain (sub-fragment 2 or S2), and the rod domain (light meromyosin [LMM]). The continuous α-helix neck and LMM domains homodimerize to form a coiled coil. Multiple coils assemble together in an ordered manner to form the thick filament, facilitated by the heptad repeat structure of the LMM domain. **(B)** Schematic representation of the MyHC-slow heptad repeat structure, denoted *a-g*. Positions *a* and *d* form a seam at the interface of the two rod/LMM helices through hydrophobic interactions, binding the rods together. The remaining residues are exposed to the cytoplasm, and therefore tend to be hydrophilic. Residues *b*, *c* and *f* mediate packing of the myosin molecules together to form the thick filament, and are commonly mutated in MSM. Binding partners such as myomesin 1, titin and slow myosin binding protein C also mediate thick filament formation **(C)** Alignment of MyHC-slow orthologues from human, pig, rat, zebrafish, lamprey, nematode, and yeast for the UK1 missense variant p.Glu1555Gly (top) and AUS1 Arg1711Trp (bottom; both highlighted in red).

and recessive myosin storage myopathy (MSM, MIM 608358, MIM 255160), Laing distal myopathy (MIM 160500), scapuloperoneal myopathy (MIM 181430) [1,2], and subgroups of congenital myopathies with characteristic histopathological features such as multi-minicores [3] and myofiber type disproportion with small type I myofibers [4].

MYH7 (MIM 160760) encodes the β-cardiac/slow skeletal myosin heavy chain (MyHC-slow), expressed predominantly in the cardiac ventricles and slow skeletal (type I) myofibers. Myosin acts as a "molecular motor" through its interaction with actin of the thin filament, which is vital for skeletal muscle force generation. Myosin heavy chains such as MyHC-slow contain three main domains from the N- to the C-terminus: the globular head domain (sub-fragment 1 or S1), the neck domain (sub-fragment 2 or S2), and the rod domain (light meromyosin [LMM]) (Fig 1A,B illustrates MyHC protein structure and assembly). Most cardiomyopathy-related *MYH7* mutations cluster in the head region, whilst skeletal muscle myopathy-associated mutations tend to occur in the rod domain, with some notable exceptions [5]. MSM mutations in particular generally cluster at the very distal end of the rod, encoded by exons 37–40 [5].

MSM is a protein aggregate myopathy characterized by sub-sarcolemmal collections of slow myosin, previously known as hyaline bodies [6–8]. Disease onset ranges from the neonatal period to adulthood, with clinical features including hypotonia, scapuloperoneal or generalized muscle weakness, and slow progression [9]. Type I myofiber predominance is a frequent but non-specific histopathological feature. Dominantly inherited MSM is rare, with fewer than 75 reported cases [9], and autosomal recessive MSM has only been reported in two families [8,10]. In the two previously reported recessive families, onset ranged from late adolescence to adulthood, with key clinical features of cardiomyopathy, proximal muscle weakness, wasting, and respiratory impairment, and with variable facial and spinal involvement, and creatine kinase elevation.

Here we describe 3 additional cases with recessive *MYH7*-related disease, expanding the clinico-pathological spectrum and aiding the diagnosis and management of this ultra-rare myopathy. We also report skinned-myofiber contractility studies, previously only performed on skeletal and cardiac muscle from patients with dominantly inherited *MYH7* mutations [11], and investigate the impact on myosin filament formation *in cellulo* as previously described [12,13], utilizing COS-7 cells transfected with an *MYH7* construct containing the Arg1712Trp mutation identified in Family AUS1.

2. Patients and methods

2.1. Patient details

Family AUS1 was a consanguineous Australian family of Middle Eastern ancestry (Fig. 2A). The parents were first cousins. The mother had two miscarriages before the birth

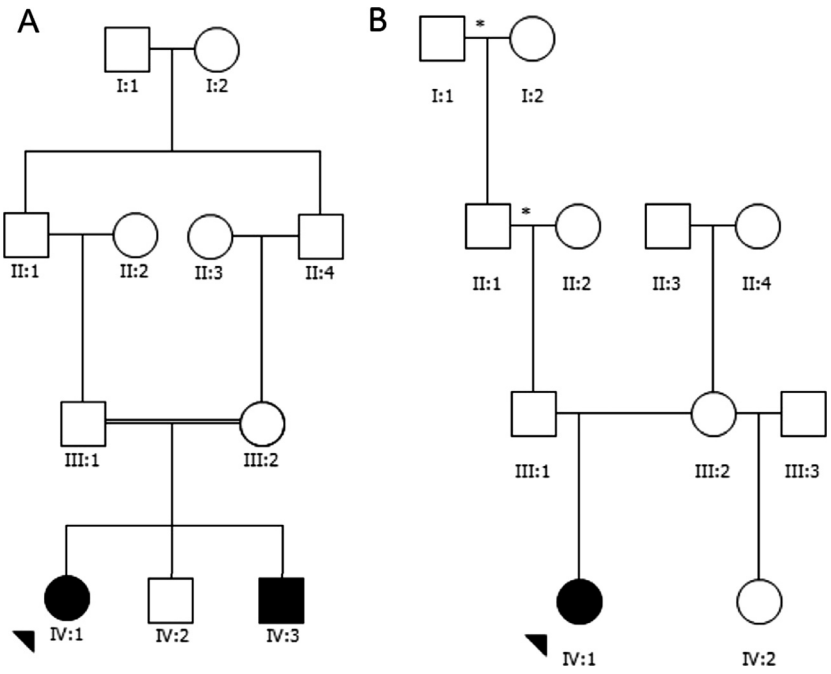

Fig. 2. Pedigrees of the two families described in this study. **(A)** Pedigree of family AUS1, a consanguineous Australian family of Middle Eastern descent. **(B)** Pedigree of family UK1, a Caucasian British family. Asterisk indicates family members that required pacemaker insertion in late adulthood.

of their eldest child. The two affected siblings were aged 21 and 13 years. There was also a healthy younger brother aged 18 years. There was no additional family history of neurological or cardiac abnormalities in other first- or second-degree family members.

Family UK1 was a non-consanguineous Caucasian family of Irish descent from the United Kingdom (Fig. 2B). The single affected individual from this family was aged 31 and was the only child to her parents, however she has a female maternal half sibling who is unaffected.

2.2. Muscle biopsy and histology

Vastus lateralis muscle biopsies had been undertaken in two affected individuals as part of their diagnostic work up. AUS1 IV:1 was biopsied at age 13 years and UK1 IV:1 was biopsied at age 9 years. Both samples had a portion of the biopsy oriented for cross-sectional histology and frozen at −80 °C according to standard procedures [14]. Haematoxylin and eosin (H&E), NADH-tetrazolium reductase and Gomori trichrome staining were performed. Myosin immunoperoxidase staining was performed on the AUS1 sample as previously described, the UK-1 tissue was no longer available for further immunohistochemical studies [14]. Samples prepared for electron microscopy from family AUS1 were fixed in buffered 2.5% glutaraldehyde and postfixed in 1% OsO_4, before being dehydrated and embedded in epon resin. A sample from patient UK1 was not available for further electron microscopy analysis.

2.3. Genetic analysis

2.3.1. Next generation sequencing

Patients AUS1 II:1 and AUS1 II:3 underwent diagnostic genetic testing on a targeted sub-exomic Illumina sequencing panel of 464 neurogenetic disease genes in the Diagnostic Genomics Laboratory at PathWest, Department of Health, Western Australia [15]. The data were analyzed using the Cartagenia software package (Agilent Technologies) as previously described [16]. Patient UK1 underwent diagnostic genetic testing through a targeted Illumina gene panel covering 32 genes previously implicated in congenital myopathies. The Alamut software package (Interactive Biosoftware) was used in used to evaluate the *in silico* predicted pathogenicity of identified variants.

2.3.2. Sanger sequencing

Bi-directional Sanger sequencing was used as previously described [16], to confirm recessive inheritance of both sets of variants.

2.4. Functional characterization

2.4.1. Cell transfection and imaging

The commercially available *MYH7* expression clone (Clone ID Hu28301C (Genscript)) produces full-length MyHC-slow protein tagged with enhanced green fluorescent protein (EGFP) at the C-terminus. This was used unaltered as the wild-type construct. Site-directed mutagenesis was used to generate the Arg1712Trp mutant. Simian kidney fibroblast cells (COS-7) cells [17] were seeded into wells of a

24-well plate (Nunc), each containing a Matrigel-coated glass coverslip (No. 1.5, Merck). Immediately after seeding, cells were transfected with wild-type or Arg1712Trp *MYH7* plasmid (Lipofectamine 3000, ThermoFisher). One hour post-transfection, the media containing transfection reagents was removed, and cells were washed with PBS before receiving new media. At 21 h, cells were fixed with 2% paraformaldehyde then mounted on glass slides. Cell media consisted of Dulbecco's Modified Eagle's Medium (ThermoFisher) supplemented with 10% fetal calf serum (Gibco) and 1% PenStrep (ThermoFisher). Images were obtained with a Nikon confocal C2/C2si microscope, using a 60x objective with oil.

2.4.2. Skinned myofiber studies

2.4.2.1. Permeabilized myofiber contractility. We adapted previously described methods to investigate myofiber contractile properties patient versus control muscle [18–20]. The temperature was kept at 20 °C using a temperature controller (ASI 825A, Aurora Scientific). In brief, small sections (2 × 2 mm) were isolated from the biopsies and glycerinated for 24 h at −20°C. Single myofibers from control subjects (average age at biopsy: 47±8 years) and patient AUS1 IV:1 were dissected from the muscle strips and clipped between aluminium foil T-clips. Myofibers were permeabilized in 1% (v/v) Triton™ X100/relaxing solution, then mounted between a length motor (ASI 315C I; Aurora Scientific, Aurora, ON, Canada) and a force transducer element (ASI 403A, Aurora Scientific) in a permeabilized myofiber apparatus (ASI 802D, Aurora Scientific) mounted on top of an inverted microscope (Axio Observer A1; Zeiss, Oberkochen, Germany). Sarcomere length was set to 2.5 μm using a using a 40x objective, high-speed VSL camera and ASI 900B software (Aurora Scientific). Myofiber length, width, and depth were measured at three points along the myofiber using a 10x objective, a prism, and a custom-made mirror mounted in the bath. Cross-sectional area was calculated with the average width and depth of the myofiber assuming an elliptical cross-section. To determine the Ca^{2+}-sensitivity of force generation and Hill slope, permeabilized single myofibers were exposed to solutions with incremental Ca^{2+}-concentration increases (note that exposure to incremental Ca^{2+}-concentrations renders similar force-pCa relations as exposure to randomly ordered Ca^{2+}-concentrations [21]. Steady-state forces were measured at each Ca^{2+}-concentration, then these steady-state values were normalized to the maximal force obtained at pCa 4.5. The force-pCa data were fitted to the Hill equation ($Y = 1 / [1 + 10^{n_H}$ (pCa - $pCa_{50})]$) [22,23]. Cross-bridge cycling kinetics were determined by imposing a rapid release-restretch protocol on an activated myofiber as described previously [24,25]. The force/stiffness ratio was determined by dividing the maximal active specific force by active stiffness. The rate of tension redevelopment (k_{TR}) was obtained by performing a bi-exponential fit through the force redevelopment curve. The resulting first-order rate constant k1 reflects the rate constants of cross bridge attachment and detachment (f_{app} and g_{app}, respectively) [26]. Active stiffness was measured by applying short-length perturbations of 0.3, 0.6, and 0.9% on the single myofibers while maximally activated, then fitting a linear curve through the data points [27] (see Fig. 3B for a typical trace). The 315C High-Speed Length Controller (Aurora Scientific) was used, which has a step change of length in 200μs and a length frequency response up to 2.4 kHz. This speed is sufficient for the stiffness measurements (similar length controller as previously used for similar experiments [28–30].

The criteria of acceptance regarding the myofiber contractility studies included: (1) preserved striation pattern (also required to set sarcomere length); (2) the force at the final pCa 4.5 had to be higher than 90% of the force during pre-activation. Each myofiber underwent two maximal activations (pCa 4.5) and five submaximal activations (pCa 7.0 – 6.0 – 5.8 – 5.6 – 5.4); (3) preserved sarcomere length in the myofibers after completion of the experimental protocol (to assure that the myofiber was well set in the clip). Applying these criteria, ∼70% of the myofiber experiments were included in the results shown. Determination of myosin heavy chain composition of measured myofibers was performed as described previously [18,31].

2.5. Statistical analysis of skinned myofiber data

The data was tested for significance by performing a mixed model analysis with a random effect for biopsies and post-hoc tests with a Bonferroni correction, after checking if the residues were normally distributed. Testing was performed using the software package SPSS Inc. (Armonk, NY, USA)

3. Results

3.1. Clinical findings

3.1.1. Family AUS1

Patient AUS1 IV:1 was born at term, following an uncomplicated pregnancy. She had mild meconium aspiration and low Apgar scores but was discharged home on day 4 of life. She was hypotonic since birth but crawled at 10 months and walked independently at 18 months of age. She had a very thin body habitus, which prompted consideration of an eating disorder before her muscle weakness was recognized at age 12 (see Table 3). She had severe restrictive lung disease requiring institution of nocturnal non-invasive ventilation very soon after presentation, at age 13, and a severe rapidly progressive scoliosis with spinal rigidity (consistent with a clinical diagnosis of "rigid spine syndrome"), requiring posterior spinal fusion at the level of the 3rd thoracic vertebra and 5th lumbar vertebra aged 15 years. She remained ambulant at the time of her spinal surgery, and was ambulant at age 21, although she used a wheelchair for longer distances. She had no ophthalmoplegia. At age 21, she showed a proximal pattern of weakness, bilaterally winged scapulae, mild weakness of neck extension and flexion, and a myopathic face with marked dolichocephaly.

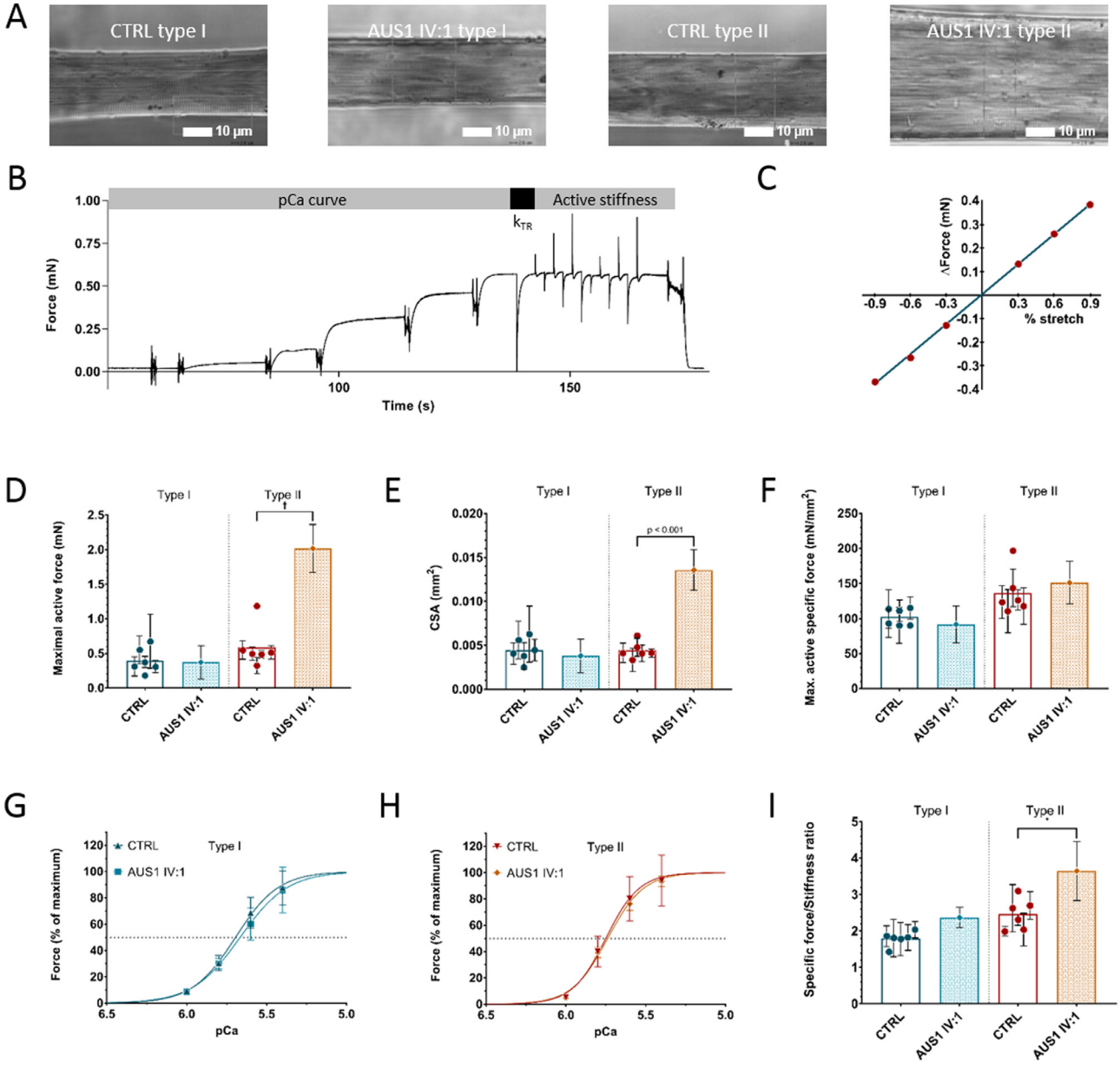

Fig. 3. Permeabilized myofiber data from control subject biopsies ($N=6$, $n=39$ for type I myofibers, $n=31$ for type II myofibers) and MYH7 patient (AUS1 IV:1: $n=9$ for type I and $n=15$ for type II myofibers). All data are depicted as mean ± SD except for panel G and H, where data is depicted as mean ± SEM. **(A)** Typical examples of permeabilized myofiber preparations isolated from a control subject (1st=type I and 3rd=type II) and the MYH7 patient (AUS1 IV:1, 2nd=type I and 4th =type II) mounted in the contractility setup. **(B)** Typical tracing showing the force response to the incremental Ca2+-concentrations, followed by the protocol in which a rapid release and restretch (kTR) and short-length perturbations (active stiffness) were imposed on the myofibers. Data shown is from a typical control myofiber (type II, CSA=0.0054mm2). **(C)** Here a typical curve is shown which is obtained after analyzing the short-length perturbations shown in panel B. This curve is fitted to a linear equation to obtain the slope, which indicate the active stiffness. **(D-F)** Absolute force, cross-sectional area (CSA) and maximal active specific force (maximal force normalized to CSA). **(G-H)** The force-pCa relation, showing the average of all type I and type II control myofibers versus the type I and type II myofibers from AUS1 IV:1. Data is depicted as mean ± SEM **(I)**. The specific force/stiffness ratio is measured to estimate the force production per cross-bridge.

Her cardiac function was normal, with the most recent cardiac assessment (including ECG and echocardiogram) having been performed at age 21 years. EMG findings were myopathic. She had normal cognition. Her creatine kinase measurements have always been within the normal range (last measurement at age 13 188 IU/l, normal range 40–240 IU/L).

Her affected younger brother, AUS1 IV:3, was 13 years of age. Pregnancy was normal. He had mild truncal weakness and difficulty running. He could walk on his toes but not his heels. He could not touch his toes due to spinal rigidity but had no scoliosis. At age 13 years, an MRI scan (Fig. 4) of the lower extremities showed marked fatty replacement of the glutei, with milder involvement of the

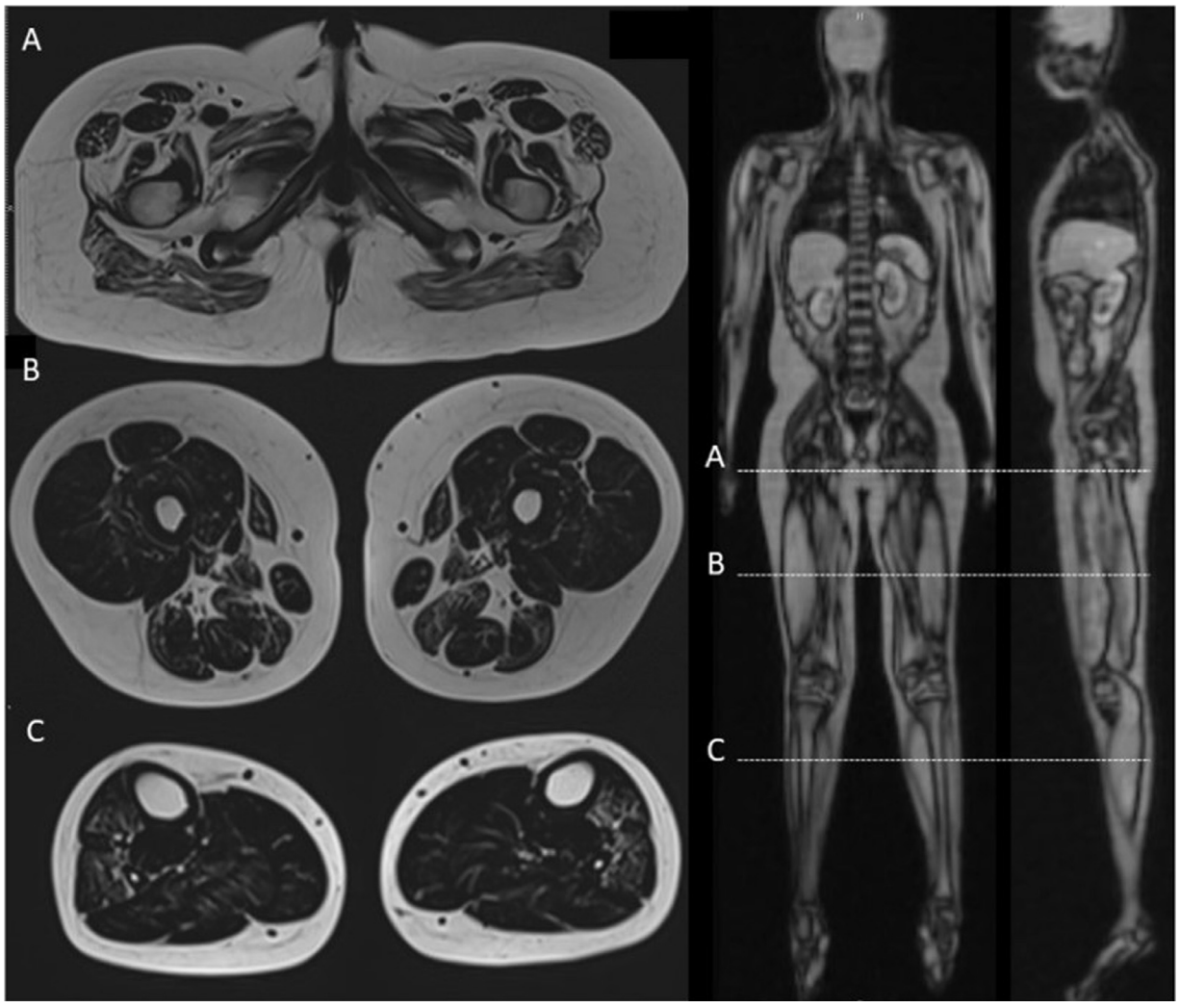

Fig. 4. MRI of Patient AUS1 IV:3 at age 13. Muscle MR T1-weighted Dixon images showing intramuscular fatty replacement in the gluteal muscles and obturators in the pelvis **(A)**; muscles of the posterior compartment of the thigh, particularly adductor magnus, semimembranosus and the long head of biceps femoris with lesser involvement of sartorius, semitendinosus and vastus intermedius and relative sparing of vastus lateralis, vastus medialis, rectus femoris and gracilis **(B)**; anterior compartment muscles of the lower leg, particularly tibialis anterior and extensor digitorum longus with sparing of the posterior compartment. **(C)**.

obturators, all compartments of both thighs, and the extensor and peroneal compartments of the lower legs, and the calf muscles bilaterally.

Lung function tests were normal at age 8. By age 12, he had developed very mild restrictive lung disease (forced vital capacity 76% predicted for age). Respiratory impairment progressed rapidly; by the age of 13 years, a nocturnal polysomnogram showed evidence of sleep-related hypoventilation, with significant desaturations and marked CO_2. On videofluoroscopy, diaphragmatic movement appeared normal. Non-invasive ventilation was initiated at 13 years of age. Creatine kinase measurements have always been in the normal range (34 IU/L in 2019).

3.1.2. Family UK1

The proband presented with toe-walking at around 15 months of age, following an uneventful pregnancy and neonatal period. She developed progressive scoliosis and required spinal fusion surgery in childhood. Marked difficulties gaining weight required gastrostomy until age 18; following gastrostomy removal, she could manage a wide range of differently textured foodstuff. She was commenced on nocturnal BiPAP ventilation in adolescence due to substantial respiratory impairment and evidence of progressive nocturnal hypoventilation. Her condition was very slowly progressive. On examination at 30 years, she was very thin with generally reduced muscle bulk. She had a rather high-pitched voice, but no other overtly myopathic facial features. She did not have ophthalmoplegia. There was proximal weakness affecting the shoulder girdle (MRC3- to MRC4) more than the hip girdle (MRC3+ to MRC4+). There was additional weakness in long finger extension (MRC3++) and ankle dorsiflexion (MRC4+). Deep tendon reflexes were generally reduced. On the most recent review, she complained about palpitations, mainly when walking but occasionally also at rest. However, cardiac examination was normal. She could

walk independently up to five minutes but had to use an electric scooter for longer distances. She could manage stairs while holding on to the banister. Although she struggled with overhead tasks, she could lift fairly heavy objects. Creatine kinase levels were within a normal range.

3.2. Muscle pathology

3.2.1. Family AUS1

3.2.1.1. Patient IV:1, age 13, vastus lateralis. Muscle biopsy showed prominent variation in myofiber size (Fig. 5A,B), with no increase in internal nuclei or split myofibers. Scattered nuclear bags were seen. There was no evidence of inflammation, nor active degeneration or regeneration. There were scattered subsarcolemmal inclusions up to 4 μm that did not stain with Periodic acid-Schiff (PAS). However, they reacted with increased intensity with myosin ATPase at pH 4.5, were pale blue on Gomori trichrome (Fig. 5A) and showed a rim of NADH-TR and glycogen. NADH-TR also revealed a moth-eaten and lobulated appearance of myofibers associated with the inclusions (Fig. 5C) in the type I myofibers. Phosphorylase was normal. The smaller myofibers were predominantly type I but the normal checkerboard pattern of myofiber typing was preserved. Immunohistochemistry showed the inclusions were reactive with slow myosin (Fig. 5D) and thus resembled hyaline bodies. Electron microscopy showed the inclusions to be composed of fine filamentous material, which appeared in part rimmed by mitochondria (Fig. 5I).

3.2.2. Family UK1

Patient IV:1, age 9, vastus lateralis

The needle muscle biopsy yielded two samples with variable pathology, both compatible with the histopathological appearance of a congenital myopathy. The first sample showed increased variability in myofiber size (Fig. 5E), with uniformity of type I myofibers on ATPase. Staining for NADH-TR and cytochrome c oxidase (Fig. 5F), however, showed some apparent myofiber type differentiation with a population of small myofibers with a prominent dark rim and slightly lobulated appearance. These myofibers had a marked moth-eaten appearance and appeared to be exclusively small type I myofibers on staining for ATPase (not shown). The second sample showed less variability in myofiber size and a more normal myofiber type distribution (Fig. 5G), although some type I myofibers appeared to be clustered with staining for ATPase. Staining for cytochrome c oxidase (Fig. 5H), however, suggested type I predominance. There were occasional small myofibers of both types with staining for ATPase. Staining for oxidative enzyme showed uneven staining but no myofibers in this area showed a clear lobulated-like appearance. There was no increase in internal nuclei, connective tissue, regenerating myofibers, no inflammatory changes or no hyaline bodies. Based on the findings, particularly of the first sample, a congenital myopathy with features of Multi-minicore Disease (MmD) was considered the most likely histopathological diagnosis,

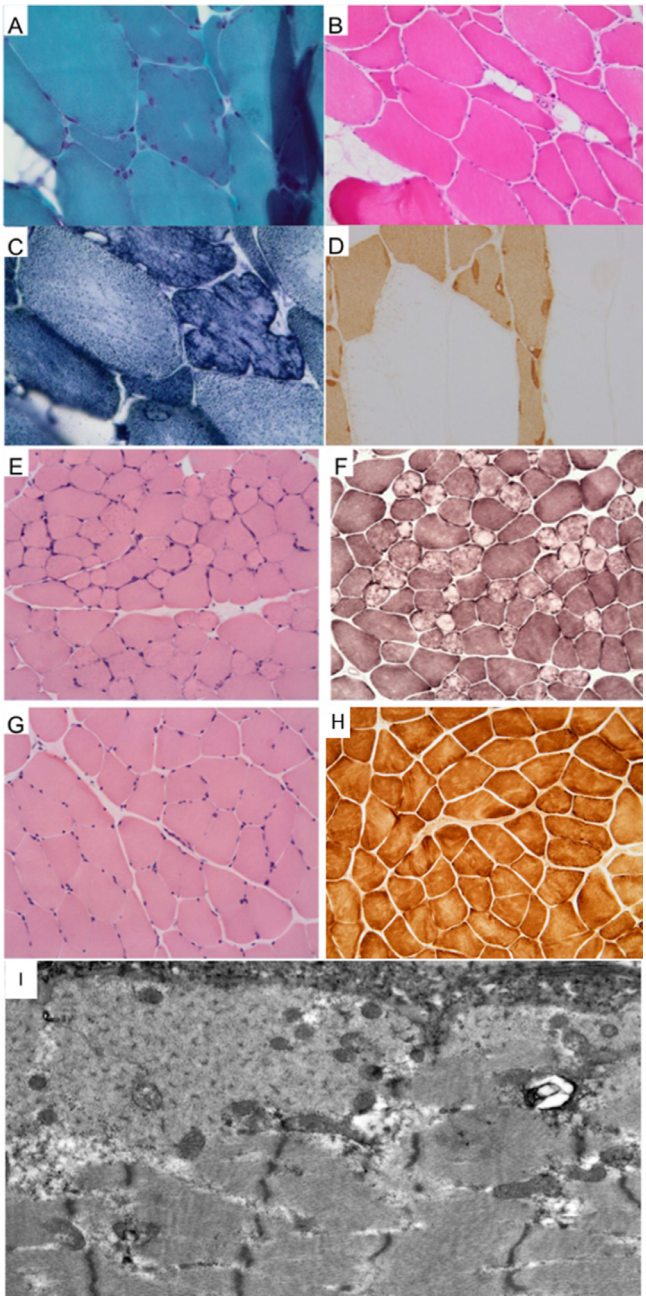

Fig. 5. AUS1 IV:1 age 13 years **(A-D, I)**. Muscle biopsy (vastus lateralis) showing prominent variation in myofiber size with fiber hypertrophy (2–117 um), with no increase in internal nuclei or split fibers. Subsarcolemmal inclusions up to 4 μm, pale blue on trichrome **(A)**, pale pink on haematoxylin and eosin **(B)**, rimmed by NADH **(C)** and immunoreactive with myosin light chain **(D)** (magnification x400). **(I)** Electron microscopy (12,000 magnification) microscopy showed the inclusions to be composed of sub-sarcolemmal fine filamentous aggregates, which appeared in part rimmed by mitochondria. UK1 IV:1 shows a population of small rounded myofibers with H&E staining **(E)** that have a dark peripheral rim, lobulated-like appearance and pronounced moth-eaten appearance with staining for cytochrome c oxidase **(F)**; in another portion of the sample H&E staining shows only mild variation in myofiber diameter **(G)**, type 1 fiber predominance and mild unevenness of stain for cytochrome c oxidase **(H)**.

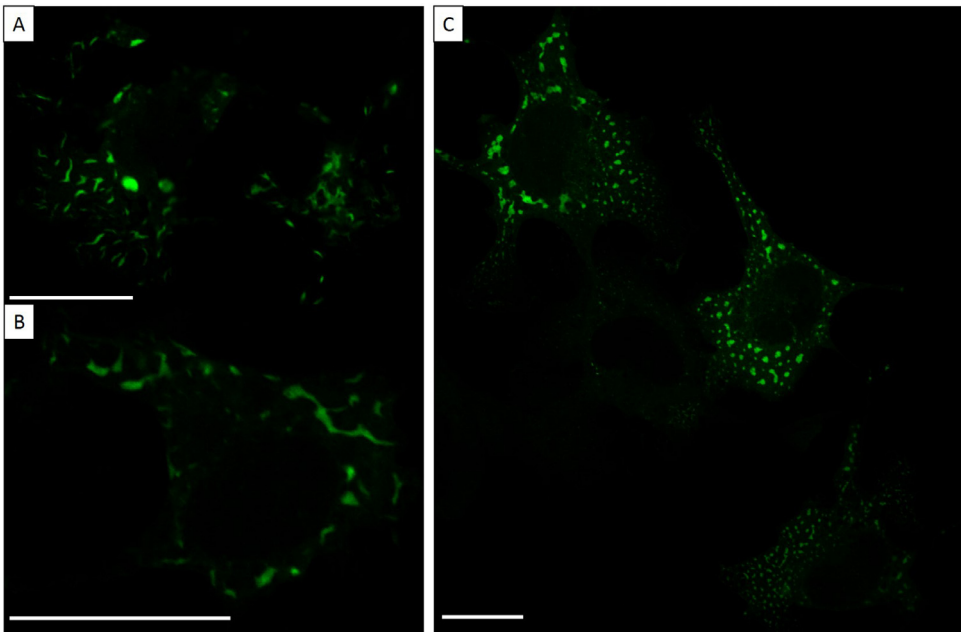

Fig. 6. Confocal microscopy images of wild-type **(A, B)** and Arg1712Trp mutant **(C)** GFP-tagged MYH7 (COS-7 cells) at 21 h post-transfection. Representative images, taken using 60x objective. The wild-type forms long filamentous assemblies. The mutant shows defective self-assembly, forming discrete foci of myosin. All scale bars represent 25 μm.

although cores could unfortunately not be confirmed on electron microscopy due to unavailability of muscle tissue.

3.3. Genetic findings

3.3.1. Family AUS1 (Australia)

The targeted neuromuscular panel revealed a homozygous missense change in *MYH7* (c.5134C > *T*, p.Arg1712Trp) in both affected siblings. Sanger sequencing showed the variant was heterozygous in each parent. DNA from the unaffected brother was not available for testing. This variant was absent in gnomAD [32] and the Greater Middle East Variome [33]. The amino acid residue is conserved to lamprey (L. *Camtschaticum*) (Fig. 1C). The variant was predicted to be deleterious by five *in-silico* prediction programs (Provean [34], SIFT [35], MutationTaster2 [36], Mutation Assessor and PolyPhen2 [37]). This residue lies in the *f* position in the rod domain coiled-coil heptad repeat (Fig. 1B). This variant was initially treated as a variant of unknown significance in a diagnostic setting (based on American College of Medical Genetics and Genomics Guidelines [38]), and was not confirmed as pathogenic until functional studies were completed.

3.3.2. Family UK1 (UK)

Genetic testing of UK1 IV:1 on a next generation sequencing congenital myopathy panel revealed compound heterozygosity for two variants in *MYH7*: c.4699C > *T*;p.Gln1567* (maternally inherited) and c.4664A > *G*; p.Glu1555Gly (paternally inherited). These are also both absent from gnomAD [32] and the Greater Middle East Variome [33]. The missense mutation affects a *c* position in the rod-domain heptad repeat (Fig. 1B). The residue is conserved to nematode (*C. Elegans)* (Fig. 1C). The combination of a truncating variant and rare, conserved missense variant allowed these two variants to be immediately classified as pathogenic [38].

3.4. Functional characterization

3.4.1. Transfection findings

At 21 h post-transfection, the EGFP-tagged MyHC-slow was distributed throughout the cytoplasm, aggregating into discrete structures. The wild-type aggregates formed long, filamentous structures (Fig. 6A, B). The Arg1712Trp mutant MyHC-slow instead formed many small, round inclusions (Fig. 6C).

3.4.2. Skinned myofiber findings

In patient AUS1 IV:1, both type I and type II myofibers displayed a well-preserved striated pattern (Fig. 3A). Type I myofibers had an absolute force, cross-sectional area (CSA) and force normalized to cross-sectional area (maximal active specific force) comparable to myofibers of control subjects (Fig. 3D–F, Table 1). Fig. 3C shows a typical curve from the active specific force protocol (see Fig. 3B) and fitted to a linear equation. Type II myofibers had higher absolute force (241%, $p < .001$) and CSA (209%, $p < 0.001$) compared to myofibers of control subjects, but maximal active specific force was comparable to controls (Fig. 3D-F, Table 2). We plotted the force-pCa relation, showing the force generated at incremental Ca^{2+} concentrations in AUS IV:1 (Fig. 3G-H).

Table 1
Data of patient (AUS1 IV:1) and control (CTRL) type I myofibers. All data are depicted as mean ± standard deviation. The number of measured biopsies (N) and single myofibers (n) is shown, as well as the percentage change (%) of patient compared to control and the associated p-value. F = absolute force; CSA = cross-sectional area; F/CSA = specific force (maximum force normalized to CSA); pCa50 = calcium sensitivity; nHill = Hill coefficient; ktr = rate constant of tension redevelopment; Active stiffness indicates the number of strongly bound cross-bridges during maximal activation; Force per cross-bridge is estimated from the specific force/stiffness ([F/CSA]/[A*ctive* S*tiffness*]) ratio.

Type I fibers							
Tissue	(mean ± SD)	CTRL	(N/n)	AUS1 IV:1	(N/n)	%	p-value
F	mN	0.399 ± 0.18	(6/39)	0.372 ± 0.241	(1/9)	−7	0.684
CSA	mm^2	0.0045 ± 0.0014	(6/39)	0.0038 ± 0.0019	(1/9)	−16	0.306
F/CSA	mN/mm^2	102.1 ± 12.3	(6/39)	91.5 ± 26.2	(1/9)	−10	0.451
pCa50	..	5.7 ± 0.02	(6/37)	5.69 ± 0.05	(1/9)	0	0.484
n_{Hill}	..	−3.26 ± 0.24	(6/37)	−2.94 ± 0.28	(1/9)	−10	0.633
k_{TR}	s^{-1}	5.59 ± 0.77	(6/37)	4.64 ± 1.14	(1/7)	−17	0.340
ActStiff	mN/mm^2	58.8 ± 6.1	(6/37)	43.4 ± 10.1	(1/7)	−26	0.068
Tension/Stiffness	ratio	1.79 ± 0.2	(6/37)	2.37 ± 0.28	(1/7)	32	0.117

Table 2
Data of patient (AUS1 IV:1) and control (CTRL) type II myofibers. All data are depicted as mean ± standard deviation. The number of measured biopsies (N) and single myofibers (n) is shown, as well as the percentage change (%) of patient compared to control and the associated p-value. F = absolute force; CSA = cross-sectional area; F/CSA = specific force (maximum force normalized to CSA); pCa50 = calcium sensitivity; nHill = Hill coefficient; ktr = rate constant of tension redevelopment; Active stiffness indicates the number of strongly bound cross-bridges during maximal activation; Force per cross-bridge is estimated by the specific force/stiffness ([F/CSA]/[A*ctive* S*tiffness*]) ratio.

Type II fibers							
Tissue	(mean ± SD)	CTRL	(N/n)	AUS1 IV:1	(N/n)	%	p-value
F	mN	0.591 ± 0.301	(6/31)	2.017 ± 0.346	(1/15)	241	<0.001
CSA	mm^2	0.0044 ± 0.0009	(6/31)	0.0136 ± 0.0023	(1/15)	209	<0.001
F/CSA	mN/mm^2	136.3 ± 31.6	(6/31)	151.2 ± 30.4	(1/15)	11	0.121
pCa50	..	5.74 ± 0.03	(6/39)	5.74 ± 0.06	(1/14)	0	0.697
n_{Hill}	..	−4.43 ± 0.88	(6/39)	−4.21 ± 0.52	(1/13)	−5	0.782
k_{TR}	s^{-1}	10.37 ± 1.86	(6/30)	12.56 ± 3.15	(1/15)	21	0.001
ActStiff	mN/mm^2	56.2 ± 6.7	(6/30)	44.3 ± 10.7	(1/15)	−21	0.151
Specific force/Stiffness	ratio	2.46 ± 0.43	(6/30)	3.65 ± 0.81	(1/15)	48	0.018

Table 3
Age, weight, height and body mass index (BMI) of controls and patients with muscle biopsy.

Biopsy information							
Biopsy	Patient ID	Mutation	Gender	Age (yrs)	Height (cm)	Weight (kg)	BMI
Control	1	N/A	Male	44	177	83	26.64
Control	2	N/A	Male	50	192	117.7	32.10
Control	3	N/A	Male	50	180	83	25.76
Control	4	N/A	Female	65	166	66.5	24.13
Control	5	N/A	Female	53	174	64	21.14
Control	6	N/A	Female	51	171	68	23.26
MYH7	AUS1 IV:1	Homozygous c.5134C>*T*; p.Arg1712Trp	Female	21	156	35.6	14.6
MYH7	UK1 IV:1	c.4699C>*T*; p.Gln1567* c.4664A>*G*; p.Glu1555Gly	Female	31	Not available	Not available	Not available

The k_{TR} of type I myofibers was similar to control values (Table 1). The k_{TR} was higher in type II myofibers (21%, $p < 0.05$) compared to that of controls (Table 2). The active stiffness normalized to CSA was similar to control values in both myofiber (Tables 1 and 2). The specific force/stiffness ratio was similar to control values in type I myofibers (Table 1), but 48% higher in type II myofibers compared to controls ($p < 0.05$, Table 2). For both the pCa50 and n_{Hill} no differences were found between patient and control myofibers (Tables 1 and 2).

4. Discussion

The spectrum of cardiac and skeletal muscle disorders due to dominant mutations in *MYH7* has rapidly expanded in recent years, but there have only been two reported families with recessive *MYH7*-related neuromuscular disease to date. Here we report three patients from two unrelated families with recessive *MYH7* mutations. We describe the consistent clinical features across both families, which contrast with the variable histopathological findings. We also describe the

path to genetic diagnosis for these families, highlighting some of the challenges associated with reliable pathogenicity ascertainment of variants identified through next generation sequencing approaches. Finally, we examine the contractile properties of skinned myofibers from patient AUS IV:4.

All three patients had a consistent clinical phenotype characterized by generalized weakness pronounced axially and proximally with some additional distal involvement, early-onset spinal rigidity with scoliosis requiring spinal fusion, and progressive respiratory impairment necessitating non-invasive ventilation despite preserved ambulation. In contrast to previously reported recessive MSM patients, none of our patients had developed any cardiac involvement at the time of the most recent assessment. Our patients also presented earlier, in infancy or early childhood, as opposed to between adolescence and mid-adulthood in the previously described families. Our findings expand the clinical phenotype of recessive *MYH7*-asociated myopathies, suggesting that those may be associated with more severe spinal involvement (encompassing both severe scoliosis and rigidity) than previously reported. Considering the severe and rapidly progressive respiratory involvement seen in both cases, we also highlight the importance of monitoring breathing disturbances particularly during sleep as an essential part of routine clinical management. Although our patients did not show any cardiac involvement to date, due to the previously recognized association of cardiomyopathy with recessive *MYH7* disease, close cardiac monitoring is strongly advisable.

The peculiar clinical phenotype in our patients, and notable absence of extraocular muscle involvement, is very similar to the features seen in Rigid Spine Muscular Dystrophy (RSMD) or Multi-minicore Disease (MmD) due to recessive mutations in *SEPN1,* encoding selenoprotein N. Indeed, *SEPN1*-related myopathy had been suspected in patients AUS1 IV:1 and UK1 IV:1 before the causative *MYH7* mutations were identified. Our findings suggest that *MYH7* mutations should be strongly considered in patients presenting with a picture of genetically unresolved RSMD or Rigid Spine Syndrome (RSS).

Both *MYH7* missense mutations in our patients have been associated with familial hypertrophic cardiomyopathy (HCM) in a heterozygous state [39,40], in keeping with the observation that autosomal dominant *MYH7* mutations may show reduced penetrance and variable expressivity [40]. Although the cardiac evaluation of patient UK1 IV:1 was normal, two paternal relatives had pacemakers inserted later in life, however, their *MYH7* mutation status could not be ascertained, and the relationship between their cardiac symptoms and the *MYH7* genotype of the index case thus remains uncertain. The Arg1712Trp variant has been previously reported to be associated with dominant HCM in one multiplex family and one isolated proband [40], and whilst there is no demonstrable cardiac dysfunction in the AUS1 family, we cannot exclude that HCM may develop in the future. Arg1712Trp may exhibit reduced penetrance in causing HCM, as evidenced by the observation that only 3/6 individuals harboring the variant had HCM in the paper where this MYH7 variant was initially reported [40]. Co-expression of wild-type myosin modulates the phenotype of *MYH7* mutants *in cellulo* [12,13], which may partially explain the different features between dominant and recessive disease in patients; further studies are required to fully characterize this phenomenon.

In contrast to the consistent clinical picture, the histopathological features were variable, both between the two subjects undergoing biopsies and, interestingly, in the two samples from the same muscle biopsy taken from a single patient (Family UK1). In particular, whilst the two recessive *MYH7* families reported so far both showed features of myosin storage myopathy (MSM) on muscle biopsy, MSM was the histopathological diagnosis only in one of the two patients biopsied (Family AUS1, Patient IV:1), bearing in mind that no specific immunohistochemistry for slow myosin and ultrastructural studies could be performed in the patient from the UK. In this patient the main pathology was multi-minicore like areas in one of the biopsies, resulting in a histopathological diagnosis of MmD, a recognized association of *MYH7* mutations [4,5].

Family AUS1 exemplifies the difficulty of interpreting genetic variants, even within known disease genes. The Arg1712Trp mutation was initially considered a variant of unknown significance (VUS) in a diagnostic genomic setting, due to its association with dominant HCM but absence of cardiomyopathy in family AUS1. Therefore, functional validation was extremely helpful to support pathogenicity in the context of suggestive clinico-pathological features and a presumed recessive mode of inheritance. Ad hoc research follow-up of VUS identified in a diagnostic genetic setting has been informative in many cases [41]. However, as diagnostic genomics is integrated into mainstream healthcare, the scale of VUS in need of further experimental clarification is likely to exceed the capacity for testing and validation on a research basis, and functional characterization of VUS may thus need to be integrated into diagnostic genomics, to ensure patients receive the best diagnostic service in future.

All MSM mutations reported to date affect residues at *b*, *c*, or *f* positions within the myosin rod heptad repeat (Fig. 1B), and both missense variants identified in our families confirm to this pattern. Mutations affecting these residues appear to disrupt the charge and steric properties required for thick filament formation, altering assembly and/or stability and causing abnormal myosin accumulation [9,10]. Wild-type myosins can self-assemble into ordered filaments in non-muscle cells, such as COS-7 [12], whilst previous studies have shown that myopathy-causing *MYH7* mutations have impaired filament assembly *in cellulo* [12,13]. We tested the hypothesis that the *MYH7* Arg1712Trp mutant would also exhibit altered filament aggregation: Indeed, whilst wild-type myosin formed long filaments throughout the cytoplasm in COS-7 cells (Fig. 6A, B) [13,42] suggestive of myosin filament bundles [42], the Arg1712Trp mutant localized to discrete foci, forming circular aggregates that were scattered throughout the cytoplasm, suggesting impaired ability to self-assemble (Fig. 6C). The morphology was similar to *MYH7*

Arg1500Pro and Leu1706Pro mutant transfected cells [13]. In the context of suggestive histopathological features, and the rarity and evolutionary conservation of the variant, we took this as sufficient evidence for Arg1712Trp being the cause of disease in Family AUS1.

We expected to observe changes chiefly in the type I skinned myofibers from AUS1 IV:1 muscle, however, all significant results were seen in type II myofibers, including higher CSA, k_{TR} and specific force/stiffness ratio's (suggesting increased force per cross-bridge) to increase overall force generation. It seems likely that these alterations may reflect a compensatory effect, however, caution is required when interpreting these data, considering that in myofiber preparations measurements of cross bridge cycling might be confounded by myofilament and myofiber-to-clip attachment compliance. Furthermore, although the myofibers included in our analyses all had intact striation patterns (see Fig. 3A for typical examples), we cannot exclude that there was subtle sarcomeric disarray that impacted on myofiber contractility. Ruling out such sarcomeric disarray would have required electron microcopy analyses of all myofibers that were used for contractility assays. Such post-contractility electron microscopy analysis of muscle fibers is unprecedented and would have been extremely challenging to conduct. Lastly, a major handicap of our study is the fact that the data are based on observations from only a single biopsy, an unavoidable consequence of the rarity of the condition under investigation.

In conclusion, we have demonstrated that recessive *MYH7* mutations cause a childhood-onset myopathy with features of the Rigid Spine Syndrome (RSS) and early-onset, rapidly progressive respiratory impairment. Although cardiac involvement was still absent in our patients, this may develop in future and must be actively monitored for. In support of its pathogenicity, we have shown that the Arg1712Trp mutation has defective localization *in cellulo*, and have highlighted possible compensatory mechanisms in type II myofibers. Our findings will help clinicians and geneticists with diagnosis, management and counselling of patients with recessive *MYH7* disease and their relatives.

Acknowledgments

We would like to thank the families for their kind participation. We thank Homa Tajsharghi for insightful comments about myosin disease mechanisms. The authors would like to thank the Genome Aggregation Database (gnomAD) and the groups that provided exome and genome variant data to this resource. A full list of contributing groups can be found at https://gnomad.broadinstitute.org/about. This study was supported by Australian National Health and Medical Research Council (NHMRC) Fellowships APP1117510 (NGL) and APP1122952 (GR), GNTAPP1090428 (EO), NHMRC Project grant APP1080587. SB was supported by The Fred Liuzzi Foundation Neuromuscular PhD Scholarship. Funding for consumables came from the Fred Liuzzi Foundation, and NHMRC.

Supplementary materials

Supplementary material associated with this article can be found, in the online version, at doi:10.1016/j.nmd.2019.04.002.

References

[1] Tajsharghi H, Oldfors A. Myosinopathies: pathology and mechanisms. Acta Neuropathol 2013;125:3–18.
[2] Klaassen S, Probst S, Oechslin E, Gerull B, Krings G, Schuler P, et al. Mutations in sarcomere protein genes in left ventricular noncompaction. Circulation 2008;117:2893–901.
[3] Cullup T, Lamont PJ, Cirak S, Damian MS, Wallefeld W, Gooding R, et al. Mutations in MYH7 cause Multi-minicore Disease (MmD) with variable cardiac involvement. Neuromuscul Disord 2012;22:1096–104.
[4] Muelas N, Hackman P, Luque H, Suominen T, Espinós C, Garcés-Sánchez M, et al. Spanish MYH7 founder mutation of Italian ancestry causing a large cluster of Laing myopathy patients. Clin Genet 2012;81:491–4.
[5] Fiorillo C, Astrea G, Savarese M, Cassandrini D, Brisca G, Trucco F, et al. MYH7-related myopathies: clinical, histopathological and imaging findings in a cohort of Italian patients. Orphanet J Rare Dis 2016;11:91.
[6] Dahl-Halvarsson M, Pokrzywa M, Rauthan M, Pilon M, Tajsharghi H. Myosin storage myopathy in C. Elegans and human cultured muscle cells. PLoS One 2017;12:1–14.
[7] Dye DE, Azzarelli B, Goebel HH, Laing NG. Novel slow-skeletal myosin (MYH7) mutation in the original myosin storage myopathy kindred. Neuromuscul Disord 2006;16:357–60.
[8] Yüceyar N, Ayhan Ö, Karasoy H, Tolun A. Homozygous MYH7 R1820W mutation results in recessive myosin storage myopathy: scapuloperoneal and respiratory weakness with dilated cardiomyopathy. Neuromuscul Disord 2015;25:340–4.
[9] Viswanathan MC, Tham RC, Kronert WA, Sarsoza F, Trujillo AS, Cammarato A, et al. Myosin storage myopathy mutations yield defective myosin filament assembly in vitro and disrupted myofibrillar structure and function in vivo. Hum Mol Genet 2017;0:1–15.
[10] Tajsharghi Homa P, Oldfors Anders P, Macleod Dominic P, Swash Michael P. Homozygous mutation in MYH7 in myosin storage myopathy and cardiomyopathy. Neurology 2007;68:962.
[11] Witjas-Paalberends ER, Ferrara C, Scellini B, Piroddi N, Montag J, Tesi C, et al. Faster cross-bridge detachment and increased tension cost in human hypertrophic cardiomyopathy with the R403Q MYH7 mutation. J Physiol 2014;592:3257–72.
[12] Feinstein-Linial M, Buvoli M, Buvoli A, Sadeh M, Dabby R, Straussberg R, et al. Two novel MYH7 proline substitutions cause Laing Distal Myopathy-like phenotypes with variable expressivity and neck extensor contracture. BMC Med Genet 2016;17:1–9.
[13] Buvoli M, Buvoli A, Leinwand LA. Effects of pathogenic proline mutations on myosin assembly. J Mol Biol 2012;415:807–18.
[14] Dubowitz V, Sewry CA, Oldfors A, Lane RJM. Muscle Biopsy: A Practical Approach. 4th ed. Elsevier; 2013.
[15] Davis M, Allcock R, Laing N. Next generation sequencing for neuromuscular disease in a diagnostic setting – The Perth custom neuromuscular gene panel 3 years on. Neuromuscul Disord 2016;26:S161.
[16] Beecroft SJ, McLean CA, Delatycki MB, Koshy K, Yiu E, Haliloglu G, et al. Expanding the phenotypic spectrum associated with mutations of DYNC1H1. Neuromuscul Disord 2017;27:607–15.
[17] Gluzman Y. SV-40 transformed simian cells support the replication of SV40 mutants. Cell 1981;23:175–82.

[18] Joureau B, de Winter JM, Conijn S, Bogaards SJP, Kovacevic I, Kalganov A, et al. Dysfunctional sarcomere contractility contributes to muscle weakness in ACTA1-related nemaline myopathy (NEM3). Ann Neurol 2018;83:269–82.
[19] Winter JMD, Joureau B, Lee EJ, Kiss B, Yuen M, Gupta VA, et al. Mutation-specific effects on thin filament length in thin filament myopathy. Ann Neurol 2016;79:959–69.
[20] Ottenheijm CAC, Buck D, De Winter JM, Ferrara C, Piroddi N, Tesi C, et al. Deleting exon 55 from the nebulin gene induces severe muscle weakness in a mouse model for nemaline myopathy. Brain 2013;136:1718–31.
[21] Lee E-J, De Winter JM, Buck D, Jasper JR, Malik FI, Labeit S, et al. Fast skeletal muscle troponin activation increases force of mouse fast skeletal muscle and ameliorates weakness due to nebulin-deficiency. PLoS One 2013;8:e55861.
[22] Hill AV. The possible effects of the aggregation of the molecules of haemoglobin on its dissociation curves. J Physiol 1910;40 iv–vii.
[23] Walker JS, Li X, Buttrick PM. Analysing force–pCa curves. J Muscle Res Cell Motil 2010;31:59–69.
[24] Malfatti E, Lehtokari V-L, Bohm J, De Winter JM, Schaffer U, Estournet B, et al. Muscle histopathology in nebulin-related nemaline myopathy: ultrastrastructural findings correlated to disease severity and genotype. Acta Neuropathol Commun 2014;2:44.
[25] Gordon AM, Homsher E, Regnier M. Regulation of Contraction in Striated Muscle. Physiol Rev 2000;80:853–924.
[26] Caremani M, Dantzig J, Goldman YE, Lombardi V, Linari M. Effect of inorganic phosphate on the force and number of myosin cross-bridges during the isometric contraction of permeabilized muscle fibers from rabbit psoas. Biophys J 2008;95:5798–808.
[27] Manders E, Bonta PI, Kloek JJ, Symersky P, Bogaard H-J, Hooijman PE, et al. Reduced force of diaphragm muscle fibers in patients with chronic thromboembolic pulmonary hypertension. Am J Physiol Lung Cell Mol Physiol 2016;311:L20–8.
[28] Chandra M, Mamidi R, Ford S, Hidalgo C, Witt C, Ottenheijm C, et al. Nebulin alters cross-bridge cycling kinetics and increases thin filament activation: a novel mechanism for increasing tension and reducing tension cost. J Biol Chem 2009;284:30889–96.
[29] Martyn DA, Smith L, Kreutziger KL, Xu S, Yu LC, Regnier M. The effects of force inhibition by sodium vanadate on cross-bridge binding, force redevelopment, and Ca2+ activation in cardiac muscle. Biophys J 2007;92:4379–90.
[30] Ochala J, Larsson L. Effects of a preferential myosin loss on Ca2+ activation of force generation in single human skeletal muscle fibres. Exp Physiol 2008;93:486–95.
[31] Ottenheijm CAC, Witt CC, Stienen GJ, Labeit S, Beggs AH, Granzier H. Thin filament length dysregulation contributes to muscle weakness in nemaline myopathy patients with nebulin deficiency. Hum Mol Genet 2009;18:2359–69.
[32] Lek M, Karczewski KJ, Samocha KE, Banks E, Fennell T, O AH, et al. Analysis of protein-coding genetic variation in 60,706 humans. Nature 2016;536:285–92.
[33] Scott EM, Halees A, Itan Y, Spencer EG, He Y, Azab MA, et al. Characterization of greater middle eastern genetic variation for enhanced disease gene discovery. Nat Genet 2016;48:1071–6.
[34] Choi Y, Chan AP. PROVEAN web server: a tool to predict the functional effect of amino acid substitutions and indels. Bioinformatics 2015;31:2745–7.
[35] Grimm DG, Azencott CA, Aicheler F, Gieraths U, Macarthur DG, Samocha KE, et al. The evaluation of tools used to predict the impact of missense variants is hindered by two types of circularity. Hum Mutat 2015;36:513–23.
[36] Schwarz JM, Cooper DN, Schuelke M, Seelow D. Mutationtaster2: mutation prediction for the deep-sequencing age. Nat Methods 2014;11:361–2.
[37] Adzhubei IA, Schmidt S, Peshkin L, Ramensky VE, Gerasimova A, Bork P, et al. A method and server for predicting damaging missense mutations. Nat Methods 2010;7:248–9.
[38] Richards S, Aziz N, Bale S, Bick D, Das S, Gastier-Foster J, et al. Standards and guidelines for the interpretation of sequence variants: a joint consensus recommendation of the American College of Medical Genetics and Genomics and the Association for Molecular Pathology. Genet Med 2015;17:405–24.
[39] Nunez L, Gimeno-Blanes JR, Rodriguez-Garcia MI, Monserrat L, Zorio E, Coats C, et al. Somatic MYH7, MYBPC3, TPM1, TNNT2 and TNNI3 mutations in sporadic hypertrophic cardiomyopathy. Circ J 2013;77:2358–65.
[40] Hougs L, Havndrup O, Bundgaard H, Køber L, Vuust J, Larsen LA, et al. One third of Danish hypertrophic cardiomyopathy patients with MYH7 mutations have mutations in MYH7 rod region. Eur J Hum Genet 2005;13:161–5.
[41] Boycott KM, Vanstone MR, Bulman DE, MacKenzie AE. Rare-disease genetics in the era of next-generation sequencing: discovery to translation. Nat Rev Genet 2013;14:681–91.
[42] Moncman CL, Rindt H, Robbins J, Winkelmann DA. Segregated assembly of muscle myosin expressed in nonmuscle cells. Mol Biol Cell 1993;4:1051–67.